Analyst

Accepted Manuscript

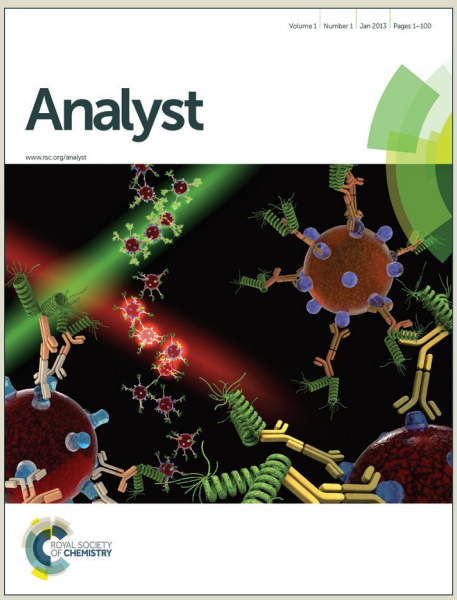

ROYAL SOCIETY OF CHEMISTRY

www.rsc.org/analyst

Analyst

RSCPublishing

ARTICLE

Imaging phosphorylated peptides distribution in human lens by MALDI MS

Cite this: DOI: 10.1039/x0xx00000x

Jing Jiao[a,b,‡], Aizhu Miao[c,‡], Ying Zhang[a,b], Qi Fan[c], Yi Lu[c] and Haojie Lu[a,b,*]

Received 00th January 2012,
Accepted 00th January 2012

DOI: 10.1039/x0xx00000x

www.rsc.org/

Phosphorylation acts vital roles in complex biological process such as cellular growth, division and signaling transduction. However, due to the low ionization efficiency of phosphorylated peptides, it is still a huge challenge to obtain region-specific phosphorylated peptides distribution by imaging mass spectrometry. To achieve the on-tissue analysis of phosphorylated peptides, we took advantage of graphene oxide-immobilized enzyme reactor to conduct the in-situ digestion, followed by dephosphorylation treatment that removed the phosphate groups thereby helped to improve the signal intensity of phosphorylated peptides. A visual representation of phosphoproteome of human lens was successfully mapped. Results showed that phosphorylated peptides localized mainly in the nuclear region of healthy lens while outer cortex is the dominant region for phosphorylated peptides of cataratous lens.

Introduction

Imaging mass spectrometry (IMS), one of the advanced technologies in mass spectrometry, allows visualizing the spatial distribution of molecules on-tissue by their molecular masses.[1-4] In this way, the relatively complex information in biological sample are exhibited in images, which are more understandable and acceptable for most people.[5] Since being proposed in 1997 by Caprioli,[6] this technology has been successfully employed for direct on-tissue analysis of drugs,[7,8] lipids,[9] metabolites,[10] and peptides and proteins.[11] Tissue sections under different physiological or pathological conditions can produce different m/z abundance patterns that might be used as diagnostic biomarkers for disease [12] such as breast cancer [13] and gastric cancer.[14]

Phosphorylation research is one of the hot spots in the field of proteomics because phosphorylation plays vital roles in biological process such as cellular growth, division, and signaling transduction. However, phosphorylated peptides are often overpowered by non-phosphorylated peptides during the mass spectrometry analysis due to the low stoichiometry and low ionization efficiency of phosphorylated peptides. As a result, in the traditional proteomics workflow, selective capture of phosphorylated proteins or phosphorylated peptides from complex mixtures is essential before MS analysis.[15,16] Nevertheless, traditional in-tube enrichment approaches are not applicable to IMS because the sample homogenization process inevitably lead to the loss of spatial distribution information. Briefly, key sample preparation steps of MALDI IMS includes tissue specimens sectioning, tissue mounting, tissue pretreatment like washing and in-situ digestion, matrix application, data acquisition, and imaging analysis. No preliminary isolation is conducted before mass spectrometry analysis. Therefore, highly abundant proteins and peptides are more readily detected. Recently, several new approaches such as utilizing proper derivatized reagents and applying suitable matrices have been reported to improve the detection of interested analytes.[17,18] However, studies using IMS for phosphorylated peptides analysis are rarely reported, which may be attributed to the lack of effective methods for generating abundant phosphorylated peptides signals in IMS. In a word, developing feasible approaches for phosphoproteome mapping is extremely urgent.

The purpose of this study is to establish an IMS workflow that can achieve visualization and comparison of the distribution of phosphorylated peptides on-tissue. We first used a highly efficient in-situ digestion platform with graphene oxide-immobilized enzyme reactor (GO-IMER) to generate peptides that have stronger ionization ability than proteins during mass spectrometry analysis.[19] Alkaline phosphatase was followed to in-situ remove phosphates group for enhancement of the ionization efficiency of phosphorylated peptides. The workflow was optimized using standard phosphorylated proteins and was finally applied to IMS analysis of human lens tissue. Human lens has unique protein composition with α-, β-, and γ-crystallins as the major components.[20] During the human lifespan, the lens loses transparency gradually and may become opaque the development of cataract.[21] The crystallins undergo many post-translational modifications including truncation, deamidation, glycation, and phosphorylation.[22] Recent advances in mass spectrometry and phosphorylated proteins/peptides enrichment allow the identification of phosphorylation sites in crystallins with high accuracy. Earlier studies have indicated that phosphorylation has physiologic significance in human eye diseases.[23,] For example, the distributions of α-crystallin phosphorylation in bovine and rabbit lenses have been

investigated.[24] Yet the present study focused on a single protein, and the high throughput of phosphorylation analysis for human lens at the peptide level was elusive. In this work, by means of the newly developed IMS workflow, the distribution of phosphorylated peptides between normal and cataractous human lenses were mapped and compared.

Experimental section

Materials and reagents

Graphene oxide powder was purchased from Nanjing XFNANO Materials Tech Co., Ltd. 2,5-Dihydroxybenzoic acid (DHB), Tosylphenylalanine chloromethyl-ketone (TPCK)-treated trypsin, alpha-casein (α-casein), beta-casein (β-casein) from bovine milk and ovalbumin from egg white, ammonium bicarbonate (ABC), acetonitrile (ACN) were purchased from Sigma Chemical (St. Louis, MO, USA). Standard peptide (LSITGTYDLK, m/z 1110.60) and standard phosphorylated peptide (EQDSEpSQTLDK, m/z 1359.53) were purchased from ChinaPeptides Co., Ltd and the purity of the peptides was more than 99%. Alkaline phosphase from calf intestinal (CIP) was purchased from New England Biolabs. Phosphoric acid (H_3PO4) was obtained from Shanghai Chemical Reagent Company, Ltd. Water was purified using a Milli-Q system (Millipore, Molsheim, France). Trifluoroacetic acid (TFA) was purchased from Merck (Darmstadt, Germany). Ethanol of analytical grade and was purchased from Shanghai Chemical Reagent Company (Shanghai, China). An aqueous solution of GO (2 mg/mL) was prepared by transferring the powder to a 1.5 mL-Eppendorf tube and suspending in water. The stock solution was stored at room temperature and used for further experiments. The trypsin was suspended in 0.1% (v/v) TFA, reaching a concentration of 2 mg mL^{-1} and was stored at -20 ºC.

Enzyme Immobilization

Trypsin was immobilized onto GO by adsorption. The details was described in an earlier research of our group.[19] In brief, trypsin solution and GO aqueous suspension were diluted in phosphate buffer (pH=5) to the desirable concentration separately. Then the two solution were incubated with each other for 10 minutes at room temperature. Before spotting onto the sections, the GO-immobilized trypsin were diluted by 25 mM ABC.

Digestion and Removal of Phosphates from Standard Proteins

Three standard phosphorylated proteins ovalbumin, α-casein and β-casein were chosen to evaluate the two enzyme strategy. The whole procedure was achieved on MALDI target to simulate the on-tissue digestion and phosphates removal. Proteins were firstly diluted in 25 mM ABC buffer (pH 8.1) to a concentration of 10 ng μL^{-1}. Then each protein solution (1 μL) was spotted on the MALDI plate and dried before follow-up processing. The GO-immobilized trypsin diluted by ABC was deposited on the MALDI plate with several cycles of aspirating and dispensing. The boiling water was utilized for trypsin inactivation. The dried digestion products were then treated by CIP, which were also diluted by 25mM ABC. During the drying process of enzyme, the phosphate groups were removed directly on the target. Finally, 1 μL DHB matrix (in 50% ACN containing 0.1% TFA, 1% H_3PO_4) was dropped and dried before mass analysis.

The Screening of Internal Standards

We employed the peaks from DHB, standard peptide (LSITGTYDLK, m/z 1110.6) and standard phosphorylated peptide (EQDSEpSQTLDK, m/z 1359.9) as the internal standard separately. Tryptic peptides of α-casein (100 ng μL^{-1}) solution and standard peptides mixture including non-phosphorylated peptide (10 ng μL^{-1}) and standard phosphorylated peptide (20 ng μL^{-1}) were prepared for further use. One μL α-casein digests was deposited on target and 15 μL on lens tissue, followed by standard peptides and matrix spraying. Imaging results of the phosphorylated peptide from α-casein (VPQLEIVPNpSAEER, m/z 1660.8) was normalized by each internal standard.

Tissue Preparation

Normal and cataractous human lenses were obtained from the eye bank of Eye and ENT Hospital of Fudan University and stored at -80 ºC. The research followed the tenets of the Declaration of Helsinki and was approved by the Ethics Committee of Eye and ENT Hospital of Fudan University. Frozen human lenses were attached to specimen chucks with the aid of a small amount of optimal cutting temperature (OCT) embedding medium. When the tissue was cryosectioned into 12-μm-thick sections at -18 ºC using a Leica cryostat (Leica CM3050S, Leica Microsystems Inc, Wetzlar, Germany), the lenses were cut in parallel with the equatorial plane but the cryostat blade never contacted the OCT in order to avoid the background interference. Then the lens tissue was mounted on the cover glass (with the thick of approximately 150 μm) and then the cover glass was immobilized on the metal MALDI plate using conductive adhesive after washing in the next step, which was similar with the operating steps in our previous study[19]. All the tissue sections in our study were from serial slices of the normal and cataract human lens tissue.

On-tissue Digestion and Removal of Phosphates

After mounting the lens slices on the glass slides, the sections were washed by 50%, 75%, and 100% ethanol respectively. This washing procedure removed the interfering species like salts and lipids and helped to form uniform matrix crystal on the section. Afterward, the lens tissue slice was immobilized on the MALDI plate by conductive adhesive. Tryptic digestion and removal of phosphate group on tissue were conducted as a slightly different way from the standard proteins. We manually coated the trypsin and CIP sequentially by spotting 15 μL enzyme solution across the tissue uniformly according to our previously reported method [19]. The MALDI plate was then placed in a home-built humidity chamber and incubated at 37 ℃ until the enzyme solution was dried. The whole process continued for 30 min for enzyme and alkaline phosphatase, respectively. DHB (in 50% ACN containing 0.1% TFA, 1% H_3PO_4) was sprayed by a pneumatic TLC sprayer on the tissue before imaging mass spectrometry analysis.

MALDI-IMS Analysis.

5800 Proteomics Analyzer (Applied Biosystems, Framingham, MA, USA) was used to perform IMS experiments by means of 4800 imaging software. Step size was set as 100 μm for standard peptides and 50 μm for lens tissues. Mass spectra were acquired in reflection mode between m/z 100 and 4000 with a Nd: YAG laser at 355 nm, a repetition rate of 400 Hz, and an acceleration voltage of 20 kV. Phosphorylated peptides distribution maps were created with the aid of BioMap (Novartis, Basel, Switzerland).

Results and discussion

Phosphorylated Peptides Signal Enhancement by Dephosphorylation Treatment.

Our previous study demonstrated that the in-situ protein digestion supported by GO-IMER possessed higher efficiency than the free enzyme digestion.[19] Therefore, GO-IMER was utilized in the present study to generate peptides on-tissue. However, highly abundant non-phosphorylated peptides still made the detection of phosphorylated peptides difficult. Therefore, on-tissue removal of phosphates was conducted subsequently to specifically improve the ionization of phosphorylated peptides. The dephosphorylation process was achieved by adding the alkaline phosphatase because this enzyme is able to remove phosphate groups from many kinds of molecules.[23, 25] To test the concept of enhancing the ionization of phosphorylated peptides, we performed GO-IMER digestion and dephosphorylation on the MALDI target directly using three standard phosphorylated proteins to optimize the procedure: α-casein, β-casein, and ovalbumin. The operating steps are described in detail in the experimental part. As the Figure 1 shows, one of the β-casein peptides at m/z 3121.9 (Figure 1a) lost four phosphate groups after CIP treatment, corresponding to the peak at m/z 2802.1 (Figure 1b). The mass shift of 319.8 corresponded to the loss of four phosphate groups, which clearly demonstrated that the on-target GO-IMER digestion and CIP dephosphorylation workflow is feasible. Analysis of ovalbumin and α-casein showed the similar results. None phosphorylated peptides of ovalbumin were detected before CIP treatment (Figure 1c). Comparatively, a dephosphorylated peptide with spectrum was detected after CIP treatment (Figure 1d). As for α-casein, a dephosphorylated peptide at m/z 1661.3 was detected with a 5-fold enhancement of S/N as compared to the corresponding phosphorylated peptide (Figure 1(e,f)). Another dephosphorylated peptide (corresponding phosphorylated peptide m/z 1952.6), which could not be observed in the mass spectrum before CIP treatment, was detected at m/z 1872.6. All the phosphorylated peptides information of the three proteins are summarized in Table S1. From the comparison, 5-10 fold S/N improvement was acquired after the dephosphorylation process, which made the identification of these phosphopeptides available. Thus, our strategy of on-target GO-IMER digestion and CIP dephosphorylation can help to enhance the detection of low-abundance phosphorylated peptides.

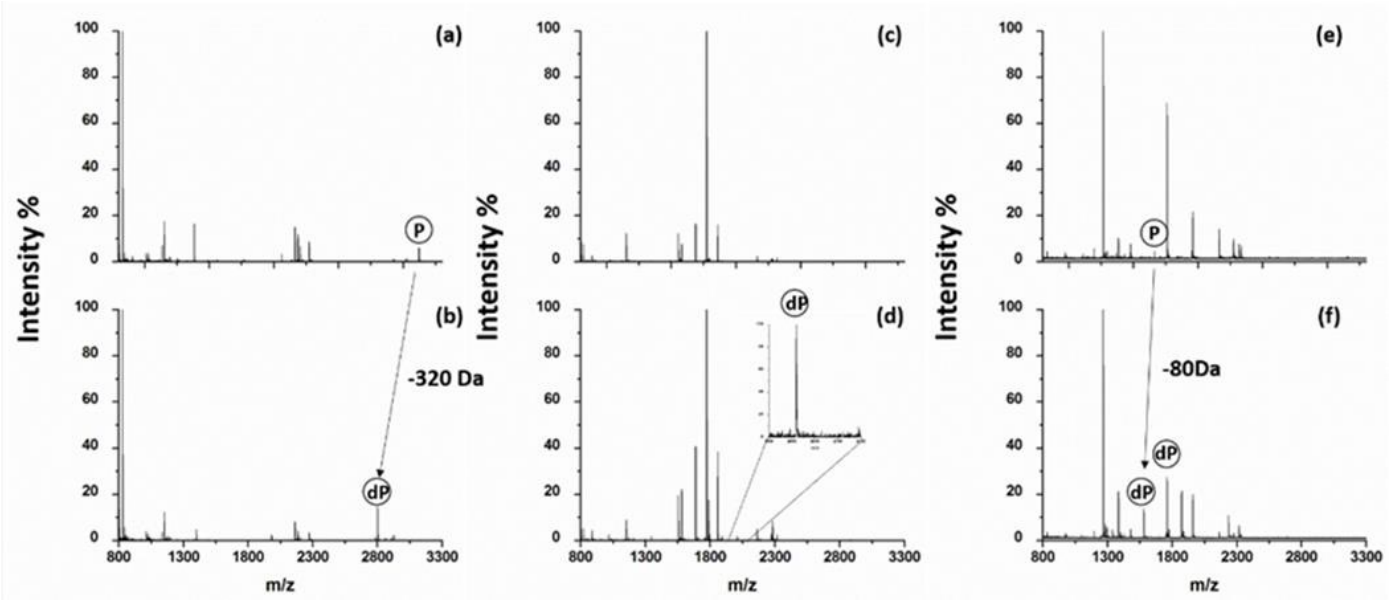

Figure 1. Mass spectra of tryptic digests of β-casein (a,b), ovalbumin (c,d) and α-casein (e,f) before (upper panel) and after (lower panel) CIP treatment. Ⓟ means the phosphorylated peptides before CIP treatment and (dP) means the dephosphorylated peptides treated by CIP. The loading amount of the three proteins is 1pmol.

The Screening of Internal Standard for Signal Normalization

Inhomogeneous crystals of matrix and analyte can introduce random variations in signal intensity during imaging mass spectrometry analysis. Signal normalization is one of the common ways to address the problem, (e.g., using known peptide covering on the tissues as an internal standard to normalize the signals). However, inhomogeneous crystals of the peptides and matrix sometimes destroyed the normalization

results. In our research, we tried to use the matrix peak and standard peptide as internal standards separately and compared the normalization results. Matrix peak at m/z 154.1 from DHB was a steady signal
during MALDI mass spectrometry analysis. We tried to use this peak, together with peaks from a standard peptide at m/z 1110.6 and a standard phosphorylated peptide at m/z 1359.9, to normalize a phosphorylated peptide at m/z 1660.8 from α-casein, to screen out the most suitable internal standard for signal normalization. The amino acid sequences of the three peptides are described in the experimental process. As displayed in Figure S1(a) and Figure S1(b), before the normalization process, the signals of the phosphorylated peptide from α-casein were detected unevenly. After normalization by matrix peak (m/z 154.1), the distribution of the same phosphorylated peptide from α-casein was more uniform than with the no-normalization treatment. In contrast, both the standard peptide (m/z 1110.6) and the standard phosphorylated peptide (m/z 1359.9) as internal standard resulted in inhomogeneous signal distribution. Besides the phosphorylated peptide of alpha-casein, we adopted three other non-phosphorylated peptides as target analytes whose information is shown in the Table S2. The peptides possessed different characteristics including aspects of amino acid sequence, m/z, and Gravy values that indicated lipophilicity. From the imaging comparison before and after DHB normalization shown in Table S2, we concluded that the normalization process correct the distribution of all the three peptides close to the truth, which implied that DHB is also applicable to non-phosphorylated peptides. In fact, during the mass spectrometry imaging analysis, the matrix crystallization was a key factor for obtaining the true distribution of the analytes. Therefore, the matrix peak was the most appropriate peak to be used as internal standard, which was used for normalization in the later experiments.

Imaging the Phosphorylated Peptides Distribution in Human Lens by MALDI-MS

Traditional phosphoproteomics enrichment and quantitative strategies have been used in human lens analysis and have revealed that phosphorylation modification may be one of the causative factors underlying the development of human cataract.[23] However, the spatial information of phosphorylated peptide within the tissue was lost due to the use of traditional homogenization method. The distribution of phosphorylated α-crystallin from human lens was visualized by IMS without digestion,[22] but this research was only focused on the α-crystallin, In the present study, in situ digestion were adopted to explore the distributional difference of phosphorylated peptides from proteins of the highest-abundance.

Figure S2 shows the mass spectra of peptides generated after on-tissue GO-IMER digestion and in-situ CIP dephosphorylation. The peak from matrix DHB was labeled with pentagram, which was used as an internal standard for IMS image normalization. We also compared the mass spectra from 'GO-IMER only' treated and GO-IMER + CIP' treated lens sections (in Figure S3). CIP treatment removed the phosphate groups from the phosphorylated peptides and increased the ionization efficiency. As the Figure S3 shows, the strongest signal peak (labeled by '*') in the mass spectrum before CIP treatment belonged to a non-phosphorylated peptides from beta-crystallin B3 (AINGTWVGYEFPGYR, m/z 1729.3). The signal of the phosphorylated peptide was too poor to be observed. However, after the CIP treatment, the two highest peaks belonged to the dephosphorylated peptides from alpha-crystallin A (TLGPFYPSR, m/z 1037.1) and alpha-crystallin B (APSWFDTGLSEMR, m/z 1496.7), respectively. Therefore, from the change of the spectra we can concluded that the CIP treatment truly increased the ionization efficiency and made the identification of phosphorylated peptides more convincing. We tried to perform the tandem mass spectrometric analysis of the phosphorylated peptides of crystallins on tissue directly, but the signals were too poor because of the low ionization efficiency and the suppression of other peptides. However, compared with the phosphorylated peptides, their dephosphorylated counterparts were more amenable to MS/MS analysis. Therefore, we performed the MS/MS spectrometric analysis of dephosphorylated peptides to confirm their identification. Figure S4 shows the MS/MS spectra of APSWFDTGLSEMR (the underline indicates the phosphorylated site) from alpha-crystallin B and TLGPFYPSR from alpha-crystallin A obtained on-tissue. We found that most of the fragment signals belonged to the corresponding peptides (as labeled on the spectra), which confirmed that CIP treatment could improve the peptide identification.

Imaging MS maps of two phosphorylated peptides from normal and cataractous lenses before and after CIP treatment are shown in Figure 2. Because of the reversibility of protein phosphorylation, one peptide can exist at the same time as two forms: peptide with phosphate group and peptide without phosphate group. Using the peptide (TLGPFYPSR) from crystallin α-A from normal tissue as an example, without CIP treatment, the phosphorylated peptides (TpLGPFYPSR) can hardly be detected (Figure 2a). By contrast, the corresponding non-phosphorylated peptide was distributed uniformly on the tissue. However, after CIP treatment, the imaging visualized the nucleus, inner cortex and middle cortex localization of peptides without phosphorylation modification. Differing from its distribution on normal lens tissue, the signals of phosphorylated peptides of crystallin α-A from cataractous lenses were detected only in the very outer cortex (Figure 2i). The above results also demonstrated that the CIP treatment helped to improve the ionization efficiency of phosphorylated peptides on-tissue without enrichment, which made it easier to recognize the distribution characteristic. We used the 'fold-change' to evaluate the signal enhancement in the standard proteins, which was truly appropriate and straight. However, for the peptides of crystallins on the tissues, the evaluation of signal enhancement was not easy because the calculation of 'fold-change' of signal intensity from each position on tissue was a tedious task. Additionally, the 'fold-change' was not uniform across the sections. Therefore, we used the colour change to reflect the signal intensity change before and after CIP treatment. We mapped the

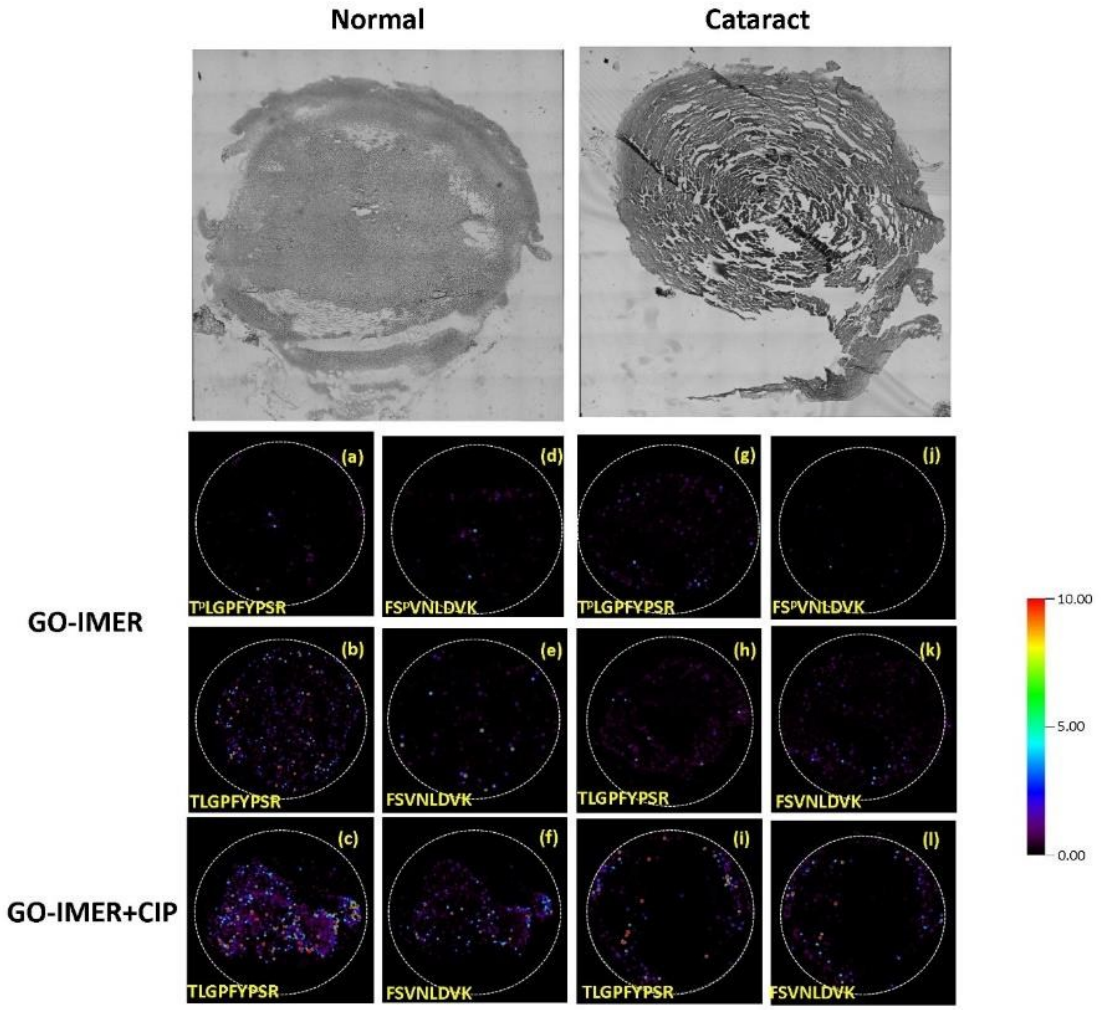

Figure 2. The comparison of phosphorylated peptides distribution between normal and cataractous lenses before and after CIP treatment. Optical images of normal and cataract lenses were shown on the top. (a)(b)(c)(g)(h)(i) display the map of a phosphorylated peptide from α-A (TLGPFYPSR, the phosphorylation site was underlined, the same below); (d)(e)(f)(j)(k)(l) display the map of a phosphorylated peptide from α-B (FSVNLDVK). The left two columns exhibit the peptides distribution of normal human lenses. The right two columns exhibit the peptides distribution of cataractous human lenses. The first line shows the distribution of peptides with phosphate group modification; the second line shows the distribution of peptides without phosphate group before CIP treatment; the third line shows the distribution of peptides without phosphate group after CIP treatment. Peptide amino acid sequence was shown in the bottom left corner.

dephosphorylated peptide distribution situation before and after CIP treatment as shown in the second line and third line of the imaging results of Figure 2. We could see that the colour distribution that represented the signals intensity distribution were not the same and that the signals of the dephosphorylated peptide after CIP treatment were more stronger than the ones before CIP treatment. For the regions of non-phosphorylated modification, the signal intensity was the same before and after CIP treatment. In contrast, in the regions with phosphorylation modification, the signal intensity became higher. Therefore, the colour change could reflect the relative content of phosphorylated peptides. Therefore, traditional imaging mass spectrometry analysis cannot reflect the reliable phosphorylation distribution, whereas an additional step of in-situ CIP dephosphorylation treatment helped to further understand the phosphorylation distribution. The distribution situation of the phosphorylated peptide from crystallin α-B was similar with that of crystallin α-A according to the IMS results. Figure S5 demonstrates the distribution of another two phosphorylated peptides from crystallin α-B and crystalllin β-S. The distribution

of phosphorylated peptides from other crystallins was consistent with the data shown in Figure 2. In general, in normal lenses the strongest signals of phosphorylated peptides from appeared in the nuclear region and inner cortex and middle cortex, while the signal of phosphorylated peptides from cataractous lenses was observed mainly in the outer cortex. This result was in accordance with previous studies. For example, Grey et al. found that the phosphorylation of alpha-crystallin A were most abundant in the lens cortex, while the non-phosphorylated peptides were located in the lens nucleus, which was accordant with our results.[26] Asomugha et al. found that α-crystallins were in low abundance in the nuclear region compared to the cortical region by laser capture microdissection[27], which were also in accord with our results. During the cataract disease development process, the change of endogenous enzyme activity leads to the final difference in peptides distribution between the normal and cataract lens.

Besides the phosphorylated peptides and de phosphorylated peptides, we also constructed the MALDI-MS map of the lens sections for a non-phosphorylated peptide before CIP treatment and after CIP treatment, as Figure S6 shows. From the imaging results, we can see that the signal intensities of the non-phosphorylated peptide were not significantly changed much before and after CIP treatment, which means that the CIP treatment would not significantly influence the ionization efficiency of non-phosphorylated peptide. The distributions of non-phosphorylated peptides in normal sections were found to be mainly in the nucleus and inner cortex, which was accordant with our previous report using GO-IMER for in situ digestion.[19]

More phosphorylated peptides were detectable when dephosphorylation was conducted by CIP on tissue than that obtained without CIP treatment. The whole phosphorylated peptides information is summarized in Table S2. A total of 23 phosphorylated peptides from 8 crystallins were detected. Most of the phosphorylated peptides concentrated in the mass range of 1000-2000 Da. The largest number of phosphorylated peptides was assigned to crystallin α-B, which exceeds one-third of the total phosphorylated peptides. One to three phosphorylated peptides could be detected in other crystallins as shown in Figure 4a. What's more, we found that phosphorylation on serine (54%) accounts for most of the phosphorylation site, followed by threonine (38%) and tyrosine (8%), as shown in Figure 4b. The distribution of identified phosphorylation sites on serine,

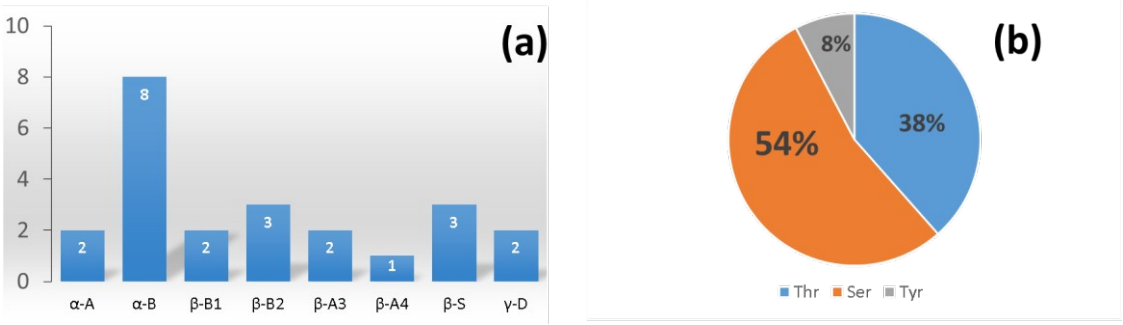

Figure 3. (a) The phosphorylated peptides numbers detected from human lenses crystallins on tissue. (b) The proportions of three phosphorylated acid residues from the detected phosphorylated peptides.

threonine, and tyrosine was in accordance with a previous report.[28]

Conclusions

Nuclear cataract was analyzed in this study. Age-related cataract is the major cause of blindness worldwide. Nuclear cataract is one of the most common forms of age-related cataract. Although the cause of cataract is not completely understood, crystallin phosphorylation has been thought to play a major role in cataractogenesis. Therefore, we focused on mapping a phosphorylation image using MS in this study. This work has provided the first phosphorylated peptides distribution maps of normal human lens and cataractous lens, which will be of interest to the lens research community. Until now, there were no other reports concerning the detection of phosphorylated peptides directly on human lens tissue. Grey and Schey et al. investigated the age-related changes in the phosphorylation distribution of α-crystallin, but phosphorylation information from only two crystallins were provided at the protein level. We have established a strategy of employing phosphatases to improve the signal of phosphopeptides by removing phosphate from peptides and to thereby measure a signal increase in MALDI imaging analysis. Phosphorylation distribution was compared between normal and cataractous human lenses, whose differences were distinguishable. The phosphorylated peptides from normal human lenses located predominantly in the nucleus, and inner and middle cortex region, whereas the phosphorylated peptides from cataractous lenses were distributed in the outer cortex. As phosphorylation is closely related with biological progress in the lenses, this approach has the potential to provide insights into phosphorylation-related human lens diseases.

Acknowledgment

The work was supported by NST (2012CB910602 and 2012AA020203), NSF (21025519 and 21335002, 21375026), the Ph.D. Programs Foundation of the Ministry of Education of China (20130071110034) and the Shanghai Projects (Eastern Scholar, 11XD1400800 and B109).

Authors Notes

*Corresponding Author
Phone: (+) 86-21-54237618. Fax: (+) 86-21-54237961. Email: luhaojie@fudan.edu.cn
[a] Shanghai Cancer Center and Key Laboratory of Glycoconjugates Research Ministry of Public Health, Fudan University, Shanghai 200032, P. R. China
[b] Institutes of Biomedical Sciences and Department of Chemistry, Fudan University, Shanghai, 200032, P. R. China
[c] Department of Ophthalmology, Eye & ENT Hospital of Fudan University, Shanghai, 200032, P. R. China
‡ Jing Jiao and Aizhu Miao contributed equally to this work

Electronic Supplementary Information (ESI) available: [details of any supplementary information available should be included here]. See DOI: 10.1039/b000000x/

References

(1) K. Chughtai and R. M. Heeren, A. *Chem. Rev.* 2010, **110**, 3237-3277.
(2) A. F. Altelaar, S. L. Luxembourg, L. A. McDonnell, S. R. Piersma and Heeren, R. M. *Nat Protoc.* 2007, **2**, 1185-1196.
(3) M. Andersson, M. R. Groseclose, A. Y. Deutch, Caprioli, R M. *Nat Methods.* 2008 **5**,101-108.
(4) M. Shariatgorji, P. Svenningsson and P. E. Andrén *Neuropsychopharmacology* 2014 **39**, 34-49.
(5) J. L. Norris and R. M. Caprioli, *Chem. Rev*. 2013, **113**, 2309-2342.
(6) R. M. Caprioli, T. B. Farmer and J. Gile *Anal. Chem.* 1997, **69**, 4751-4760.
(7) X. Liu, J. L. Ide, I. Norton, M. A. Marchionni, M. C. Ebling, L. Y. Wang, E. Davis, C. M. Sauvageot, S. Kesari, K. A. Kellersberger, M. L. Easterling, S. Santagata, D. D. Stuart, J. Alberta, J. N. Agar, C. D. Stiles and N. Y. Agar *Sci Rep.* 2013, **3**, 2859.
(8) R. Vismeh, D. J. Waldon, Y. Teffera and Z. Zhao, *Anal Chem.* 2012, **84**, 5439-5445.
(9) P. Sjovall, J. Lausmaa and B. Johansson, *Anal Chem.* 2004, **76**, 4271-4278.
(10) D. Miura, Y. Fujimura and H. Wariishi, *J. Proteomics.* 2012, **75**, 5052-5060.
(11) B. Cillero-Pastor and R. M. A. Heeren, *J.* Proteome Res. 2014, **13**, 325-335.
(12) K. Schwamborn, *J. Proteomics.* 2012, **75**, 4990-4998.
(13) S. Rauser, C. Marquardt, B. Balluff, S. O. Deininger, C. Albers, E. Belau, R. Hartmer, D. Suckau, K. Specht, M. P. Ebert, M. Schmitt, M. Aubele, H. Höfler and A. Walch, *J. Proteome Res.* 2010, **9**, 1854-1863.
(14) B. Balluff, S. Rauser, S. Meding, M. Elsner, C. Schöne, A. Feuchtinger, C. Schuhmacher, A. Novotny, U. Jütting, G. Maccarrone, H. Sarioglu, M. Ueffing, H. Braselmann, H. Zitzelsberger, R. M. Schmid, H. Hofler, M. P. Ebert, A. Walch, Am. *J. Pathol.* 2011, **179**, 2720-2729.
(15) W. F. Ma, Y. Zhang, L. L. Li, L. J. You, P. Zhang, Y. T. Zhang, J. M. Li, M. Yu, J. Guo, H. J. Lu, C. C. Wang, *ACS Nano.* 2012, **6**, 3179-3188.
(16) W. F. Ma, Y. Zhang, L. L. Li, Y. T. Zhang, M. Yu, J. Guo, H. J. Lu and C. C. Wang *Adv. Funct. Mater.* 2013, **23**, 107-115.
(17) A. Chacon, I. Zagol-Ikapitte, V. Amarnath, M. L. Reyzer, J. A. Oates, R. M. Caprioli and O. Boutaud, J. Mass Spectrom. 2011, **46**, 840-846.
(18) C. Meriaux, J. Franck, M. Wisztorski, M. Salzet and I. Fournier, *J. Proteomics.* 2010, **73**, 1204-1218.
(19) J. Jiao, A. Z. Miao, X. Y. Zhang, Y. Cai, Y. Lu, Y. Zhang and H. J. Lu, *Analyst.* 2013, **138**, 1645-1648.
(20) H. Bloemendal, W. de Jong, R. Jaenicke, N. H. Lubsen, C. Slingsby and A. Tardieu *Prog. Biophys. Mol. Biol.* 2004, **86**, 407-485.
(21) L. Takemoto and C. M. Sorensen *Exp. Eye Res.* 2008, **87**, 496-501.
(22) P. G. Hains and R. J. Truscott *J. Proteome Res.* 2007, **6**, 3935-3943.
(23) C. H. Huang, Y. T. Wang, C. F. Tsai, Y. J. Chen, J. S. Lee and S. H. Chiou *Mol. Vis.* 2011, **17**, 186-198.
(24) A. C. Grey and K. L. Schey *Mol. Vis.* 2008, **14**, 171-179.
(25) Y. Ishihama, F. Y. Wei, K. Aoshima, T. Sato and J. Oda. Kuromitsu *J. Proteome Res.* 2007, **6**, 1139-1144.
(26) A. C. Grey and K. L. Schey, *Invest. Ophthalmol. Vis. Sci.* 2009, **50**, 4319-4329.
(27) C. O. Asomugha, R. Gupta and O. P. Srivastava *Mol Vis.* 2010, **16**, 476-494.
(28) Z. Wang, J. Han, L. L. David and K. L. Schey, *Vis. Sci.* 2013, **54**, 1135-1143.